JCTC Journal of Chemical Theory and Computation

Theoretical Characterization of a Tridentate Photochromic Pt(II) Complex Using Density Functional Theory Methods

Jay C. Amicangelo*

School of Science, Penn State Erie, The Behrend College, 4205 College Drive, Erie, Pennsylvania 16563-0203

Received June 26, 2007

Abstract: Density functional theory methods have been used to characterize a tridentate photochromic Pt(II) complex [Pt(AAA)Cl], its acetonitrile complex [Pt(AAA)Cl·CH_3CN], and the transition state in the complexation reaction. B3LYP/6-31G* (effective core potential for Pt) optimized geometries of Pt(AAA)Cl and Pt(AAA)Cl·CH_3CN are found to be in reasonably good agreement with most of the applicable parameters for the available experimental crystal structures of Pt(AAA)Cl and a Pt(AAA)Cl-triphenylphoshine complex, with the exception of one of the dihedral angles, the deviation of which is determined to be due to a steric cis versus trans effect. Vibrational frequencies are calculated for Pt(AAA)Cl and *cis*-Pt(AAA)Cl·CH_3CN, and the predicted shift in the benzaldehyde carbonyl frequency is found to be in line with that observed experimentally. Singlet vertical excitation energies are calculated for Pt(AAA)Cl and *cis*-Pt(AAA)-Cl·CH_3CN using time-dependent density-functional theory and are found to be in good agreement with the experimental transition energies, although for *cis*-Pt(AAA)Cl·CH_3CN, the calculations suggest a reassignment of the experimental S_1 and S_2 transitions. Single point energies are calculated at the B3LYP/6-311+G(2d,2p) level (effective core potential for Pt) and the calculations predict the complexation reaction (dark reaction) to be exothermic and, after a correction to the entropy, to be exoergic at 298 K and to proceed with a reasonable activation energy. Based on singlet and triplet vertical excitation energies, it is speculated that the photoreaction occurs via an intersystem crossing from S_1 to T_1 for *cis*-Pt(AAA)Cl·CH_3CN followed by an adiabatic reaction along the T_1 surface and then nonradiative intersystem crossing to the S_0 state of Pt(AAA)Cl.

Introduction

Photochromism is generally defined as a reversible photo-induced transformation of a chemical species between two forms having distinct absorption spectra.[1] The majority of the studies on photochromic compounds have been for organic systems,[2] with a smaller amount of work being focused on inorganic compounds.[3] Within the inorganic systems, an even smaller amount has been concerned with transition-metal compounds and complexes.[4,5]

One particularly interesting example of a photochromic transition-metal compound is a Pt(II) complex, known as *cis*-[N-(*o*-aminobenzylidene)anthranilaldehydato-*O*,*N*,*N*′]-chloroplatinum or Pt(AAA)Cl, that was synthesized and characterized by Mertes and co-workers.[6,7] Structurally, this compound is a complex between Pt(II) and a tridentate ligand that is a Schiff base condensate of *o*-aminobenzaldehyde (Figure 1). Shortly after the initial report about the structural characterization of Pt(AAA)Cl appeared in the literature,[6] Mertes and co-workers reported that this complex underwent a reversible, photochromic solvolysis reaction, shown in Figure 1, in coordinating solvents such as acetonitrile and dimethylsulfoxide.[7] The unusual feature about this photochromic reaction was that it was appeared to operate in a reverse fashion to that observed for most other photochemical and photochromic transition-metal solvolysis reactions,[8] in that the solvolysis reaction was the reaction occurring in the

* Corresponding author e-mail: jca11@psu.edu.

10.1021/ct700158g CCC: $37.00
Published on Web 10/04/2007

dark and the recoordination of the ligand (aldehyde group) was the photoactive reaction. The primary physical evidence for the proposed photochromic solvolysis reaction (Figure 1) was a red-shift of the aldehyde carbonyl stretching frequency upon uncoordination of the aldehyde and a blue-shift in the visible absorption spectrum upon solvent coordination. Due to the instability of the solvated complex [Pt(AAA)Cl·S] upon evaporation of the solvent, Mertes and co-workers were unable to obtain a crystal structure for the acetonitrile or dimethylsulfoxide complexes.[9] However, these researchers were able to obtain a crystal structure of a related complex with triphenylphoshine, Pt(AAA)Cl·PPh_3,[10] whose infrared and visible spectral characteristics agreed with the acetonitrile and dimethylsulfoxide systems, supporting the proposed reaction.

With the ease of use and availability of computational chemistry software packages and the fast computational speed afforded by modern computers, additional support of a reaction mechanism or molecular structures can often now be obtained by high level theoretical calculations.[11] Particularly relevant to transition-metal systems was the development of reliable density functional theory methods (DFT).[12,13] In this paper, the photochromic solvolysis reaction of Pt(AAA)Cl with acetonitrile is theoretically characterized (geometries, vibrational frequencies, singlet and triplet vertical excitations, and single point energies) with density functional theory methods using the B3LYP hybrid functional.[14,15] The primary motivation for this work is the preliminary, unpublished results of Jircitano and co-workers,[16] in which the rate constants for the acetonitrile dark reaction of F, Cl, and CH_3 substituted Pt(AAA)Cl derivatives (substituted on the aromatic rings) have been measured and found to display the trend that electron withdrawing groups increased the rate and electron donating groups decreased the rate relative to Pt(AAA)Cl. It was thought that this might be due to changes in the activation energy with the substituents for the solvolysis reaction and that density functional theory calculations may be able to lend theoretical support to this idea. However, prior to embarking on density functional theory calculations for a whole series of Pt(AAA)Cl derivatives, a full theoretical characterization of Pt(AAA)Cl and its photochromic solvolysis reaction was undertaken, and this comprises the material described in this paper.

Computational Details

All theoretical calculations were carried out using the Gaussian 98[17] or Gaussian 03[18] suite of programs. Because the standard basis sets available in Gaussian 98 or Gaussian 03 are not developed for use with Pt, the Hay-Wadt (HW) relativistic effective core potential (ECP) and valence basis set,[19] modified for use with cations,[20] was used for Pt in all calculations. For all other atoms, the standard Gaussian basis sets were used. In the following descriptions and throughout the paper, only the method and standard basis sets will generally be listed, with the implicit understanding that the modified HW ECP was used for Pt in all calculations.

Ground-state geometry optimizations were performed in a series of steps with basis sets of increasing size for all atoms except Pt, involving the following general sequence:

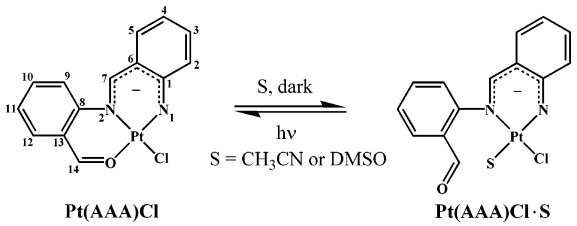

Figure 1. Structure of Pt(AAA)Cl and a schematic representation of its reversible, photochromic solvolysis reaction. The numbering scheme for Pt(AAA)Cl is the same as that used by Mertes and co-workers for the Pt(AAA)Cl crystal structure[6] and is as follows: the nitrogens are labeled as N(1) and N(2) and the carbons are labeled as C(1)−C(14).

HF/STO-3G → HF/3-21G → HF/6-31G* → B3LYP[14,15]/6-31G*. For Pt(AAA)Cl, the input geometry was that of the crystal structure reported by Mertes and co-workers[6] for the heavy atoms, with the hydrogen atoms added at standard positions using the GaussView[21] program. For the Pt(AAA)Cl·S complexes (S = CH_3CN or PH_3), most of the input geometry for the heavy atoms was taken from the crystal structure of a triphenylphosphine complex of Pt(AAA)Cl reported by Jircitano, Rohly, and Mertes,[10] except that the triphenylphosphine was replaced with a CH_3CN or a PH_3 ligand at the appropriate position (cis or trans) and again the hydrogens were added at standard positions. For the *cis*-Pt(AAA)Cl·CH_3CN transition state, the optimized *cis*-Pt(AAA)Cl·CH_3CN geometry was manipulated until an initial geometry was found that had a large negative frequency that appeared to correspond to the desired reaction coordinate. This geometry was then used as the input geometry for the transition-state optimization using the Gaussian opt=TS keyword. The NoEigenTest option to the opt keyword was used for the first step in the optimization (HF/STO-3G level), due to the presence of several other small negative frequencies for the input structure. Once the HF/STO-3G optimization was complete, a frequency analysis was performed, and this confirmed that the structure was indeed a transition state with only one negative frequency. The HF/STO-3G optimized transition-state geometry was then used as the input for the remaining series of optimizations at successively higher levels of theory, with a frequency analysis being performed at each level to confirm the optimized structure was a transition state. Single point energies were calculated at the B3LYP/6-311+G(2d,2p) level using the B3LYP/6-31G* optimized geometries and were corrected for zero-point and thermal energies using scaled B3LYP/6-31G* vibrational frequencies (scaling factor = 0.9804[22]). Singlet and triplet vertical excitation energies were calculated for the B3LYP/6-31G* optimized geometries using time-dependent density-functional theory (TDDFT), as implemented in Gaussian 98 and Gaussian 03,[23] primarily with the B3LYP functional and the 6-31+G*, 6-311+G*, and the 6-311+G(2d,2p) basis sets.

Results and Discussion

Optimized Geometries. B3LYP/6-31G* optimized geometries were obtained for the Pt(AAA)Cl and Pt(AAA)Cl·CH_3-

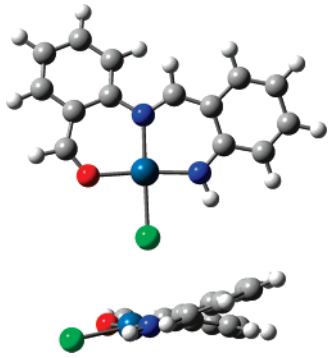

Figure 2. Optimized structure of Pt(AAA)Cl calculated using the B3LYP functional and the 6-31G* basis set on the C, O, N, Cl, and H atoms and a modified Hay-Wadt ECP on the Pt atom. The view in the lower panel is from the right side of the upper panel to emphasize the canting angle between the two ring systems. Color scheme: carbon is gray, hydrogen is white, nitrogen is blue, oxygen is red, chlorine is light green, and platinum is teal.

CN complexes and for the *cis*-Pt(AAA)Cl·CH_3CN transition state. In the case of the Pt(AAA)Cl·CH_3CN complex, an optimized geometry was obtained for the configuration in which the CH_3CN group was cis to the benzaldehyde as well as for the configuration in which the CH_3CN group was trans to the benzaldehyde. As will be discussed below, this was primarily done to assess the effect of the CH_3CN orientation on the dihedral angle of the benzaldehyde group relative to the platinum square plane, due to a significant deviation in this dihedral angle between the calculated *cis*-Pt(AAA)Cl·CH_3CN geometry and that of the X-ray crystal structure of a *trans*-triphenylphosphine adduct of Pt(AAA)Cl (abbreviated as Pt(AAA)Cl·PPh_3).[10] To further examine this effect and examine the effect of the identity of the ligand itself, cis and trans optimized geometries were also obtained for a model compound of Pt(AAA)Cl·PPh_3 in which a PH_3 group was used in place of the triphenylphosphine group, Pt(AAA)-Cl·PH_3. For all of the complexes theoretically examined in this study, the calculated bond lengths and bond angles of the tridentate *N*-(*o*-aminobenzylidene)anthranilaldehydato ligand itself were found to be in very good agreement with the values from the Pt(AAA)Cl and Pt(AAA)Cl·PPh_3 crystal structures.[6,10] Therefore, the discussion that follows will be focused primarily on the geometry around the platinum.

The B3LYP/6-31G* optimized geometry of the Pt(AAA)-Cl complex is shown in Figure 2, and selected values of the bond lengths, bond angles, and dihedral angles are listed in Table 1, along with the values determined by X-ray crystallography by Mertes and co-workers.[6] As can be seen in Figure 2 and Table 1, the approximate square planar coordination around the platinum in the Pt(AAA)Cl complex is reproduced fairly well by the optimized geometry as compared to the crystal structure. This is evidenced by a mean absolute deviation of 0.05 ± 0.02 Å between the experimental and theoretical bond lengths and a mean absolute deviation of 1.7 ± 1.1° between the experimental and theoretical bond angles. These can be reasonably compared to the average uncertainties for the bond length and bond angle parameters of the crystal structure listed in Table 1, which are 0.01 Å and 0.6°, respectively. Another feature of the complex that is well reproduced by the calculations is the significant nonplanarity (canting) between the two chelate ring systems, as can be seen in the lower panel of Figure 2. The canting angle between the chelate rings can be approximated by 180° minus the C(7)−N(2)−C(8)−C(13) dihedral angle, and this is found to be 24° for the crystal structure and 23.0° for the optimized geometry.

The B3LYP/6-31G* optimized geometry of the *cis*-Pt-(AAA)Cl·CH_3CN complex is shown in Figure 3, and selected values of the bond lengths, bond angles, and dihedral angles are listed in Table 1. A crystal structure has not been obtained for the Pt(AAA)Cl·CH_3CN complex; however, as mentioned above, Mertes and co-workers were able to determine a crystal structure for a triphenylphosphine adduct of Pt(AAA)-Cl,[10] and selected values of the experimental bond lengths, bond angles, and dihedral angles for the Pt(AAA)Cl·PPh_3 complex are listed in Table 1. It should be noted that the experimentally observed configuration of the PPh_3 is trans to the benzaldehyde group in the Pt(AAA)Cl·PPh_3 complex. The reason for this was thought to be due to unfavorable steric interactions between the PPh_3 and the benzaldehyde group.[10] Therefore, a direct comparison of all of the experimental geometric parameters of the Pt(AAA)Cl·PPh_3 complex with the calculated parameters for the *cis*-Pt(AAA)-Cl·CH_3CN complex is not possible, and only the most appropriate values are compared in Table 1.

As can be seen from Figure 3 and Table 1, the approximate square planar coordination around the platinum for the *cis*-Pt(AAA)Cl·CH_3CN complex is retained, with the acetonitrile group is acting as the fourth ligand. The calculated Pt−Cl, Pt−N(1), and Pt−N(2) bond lengths are in reasonable agreement with those for the Pt(AAA)Cl·PPh_3 complex, with deviations of 0.035, 0.02, and 0.01 Å, respectively. In terms of bond angles about the platinum, only the N(1)−Pt−N(2) angle can be compared to an experimental value, and it is in reasonable agreement with the experimental value, with a deviation of 1.2°. The largest discrepancy with the experimental Pt(AAA)Cl·PPh_3 structure appears to be with the angle between the two chelate rings, as judged by comparing the C(7)−N(2)−C(8)−C(13) dihedral angles of 93.3° and 69.1° for the experimental and calculated structures, respectively. With respect to the platinum square plane, these dihedral angles put the benzaldehyde ring at approximate angles of 87° and 111° for the experimental and calculated structures, respectively. Since the *cis*-Pt(AAA)Cl·CH_3CN optimization started with the C(7)−N(2)−C(8)−C(13) dihedral angle at the Pt(AAA)Cl·PPh_3 crystal structure value and optimized to the smaller value, it is clear that a dihedral angle near 90° is not a geometric minimum for the cis structure. This large deviation in the C(7)−N(2)−C(8)−C(13) is also the reason for the large deviation between the experimental and calculated Pt−O distance, 0.47 Å. One possibility for this large deviation could be that the cis orientation of the CH_3CN ligand causes more steric repulsions with the benzaldehyde ring, resulting in an increased dihedral angle to relieve these repulsive interactions, as opposed to the trans configuration of the PPh_3 ligand, which would not have these repulsive interactions.

Table 1. Selected Bond Lengths (Å), Bond Angles (deg), and Dihedral Angles (deg) for Pt(AAA)Cl, *cis*- and *trans*-Pt(AAA)Cl·CH_3CN, and *cis*- and *trans*-Pt(AAA)Cl·PH_3 Optimized Using Density Functional Theory and for Pt(AAA)Cl and *trans*-Pt(AAA)ClPPh_3 Determined by X-ray Crystallography

	Pt(AAA)Cl		Pt(AAA)Cl·L (L = CH_3CN or PH_3)				
parameter[a]	crystal[b]	theory[c]	*trans*-PPh_3 crystal[d]	*cis*-CH_3CN theory[c]	*trans*-CH_3CN theory[c]	*cis*-PH_3 theory[c]	*trans*-PH_3 theory[c]
			Bond Lengths				
Pt−Cl	2.309 (5)	2.37	2.355 (6)	2.39	2.41	2.40	2.42
Pt−N(1)	1.93 (2)	1.96	2.00 (1)	1.98	2.01	2.01	2.01
Pt−N(2)	1.99 (1)	2.06	2.07 (1)	2.06	2.03	2.06	2.08
Pt−N_{Ac}				2.02	2.00		
Pt−P			2.274 (6)			2.31	2.27
Pt−O[e]	2.01 (1)	2.04	3.72 (1)	4.19	3.67	4.19	3.60
			Bond Angles				
Cl−Pt−N(1)	87.0 (5)	86.6		87.0		87.0	
N_{Ac}−Pt−N(1)					90.2		
P−Pt−N(1)			92.5 (3)				93.1
N(1)−Pt−N(2)	93.6 (7)	92.5	89.2 (4)	90.4	90.4	89.5	89.7
N(2)−Pt−O	94.4 (6)	92.5					
N(2)−Pt−N_{Ac}				95.2			
N(2)−Pt−P						99.7	
N(2)−Pt−Cl			91.8 (4)		93.8		94.4
O−Pt−Cl	85.1 (4)	88.4					
N_{Ac}−Pt−Cl				87.5	85.5		
P−Pt−Cl			86.7 (2)			83.9	81.7
Pt−N_{Ac}−C_{Ac}				171.6	173.7		
			Dihedral Angles				
C(6)−C(7)−N(2)−C(8)	172 (2)	168.8	176[f]	176.4	179.3	170.7	179.6
C(7)−N(2)−C(8)−C(13)	156 (2)	157.0	93[f]	69.1	90.0	70.1	93.6

[a] Numbering scheme corresponds to that shown in Figure 1; N_{Ac} and C_{Ac} refer to the nitrogen and first carbon of the acetonitrile group, respectively. [b] Reference 6; the number in parentheses is the uncertainty in the last digit. [c] Calculations performed using the B3LYP functional and the 6-31G* basis set on the C, O, N, Cl, P, and H atoms and a modified Hay-Wadt ECP on the Pt atom. [d] Reference 10; the number in parentheses is the uncertainty in the last digit. [e] Distance between the oxygen and platinum atoms. [f] Not reported by Mertes and co-workers in ref 10; determined by examining the Pt(AAA)Cl PPh_3 crystal structure in GaussView.

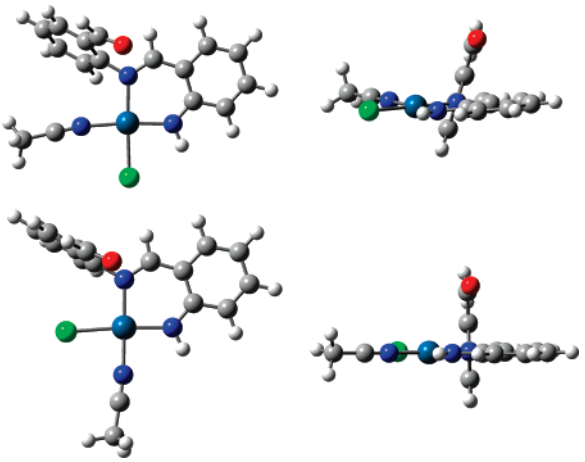

Figure 3. Optimized structure of *cis*-Pt(AAA)Cl·CH_3CN (upper) and *trans*-Pt(AAA)Cl·CH_3CN (lower) calculated using the B3LYP functional and the 6-31G* basis set on the C, O, N, Cl, and H atoms and a modified Hay-Wadt ECP on the Pt atom. The right panel in both upper and lower is the view along the N(2)−C(8) bond to emphasize the C(7)−N(2)−C(8)−C(13) dihedral angle. The color scheme is the same as that in Figure 2.

To assess if the large deviation of the C(7)−N(2)−C(8)−C(13) dihedral angle is due to the inverted configuration of the Pt(AAA)Cl·PPh_3 crystal structure as compared to that for the calculated structure of *cis*-Pt(AAA)Cl·CH_3CN, an optimization was performed for the Pt(AAA)Cl·CH_3CN complex with the CH_3CN trans to the benzaldehyde group. The B3LYP/6-31G* optimized geometry of the *trans*-Pt(AAA)Cl·CH_3CN complex is shown in Figure 3, and selected values of the bond lengths, bond angles, and dihedral angles are listed in Table 1. As can be seen in Table 1, the approximate square planar coordination around the platinum for this complex is still retained in this configuration. The calculated Pt−Cl, Pt−N(1), and Pt−N(2) bond lengths are again in reasonable agreement with those for the Pt(AAA)Cl·PPh_3 complex, with deviations of 0.055, 0.01, and 0.04 Å, respectively. Two of the bond angles about the platinum, N(1)−Pt−N(2) and N(2)−Pt−Cl, can be compared to experimental values, and the calculated angles are both in reasonable agreement with the experimental values, with deviations of 1.2° and 2.0°, respectively. The C(7)−N(2)−C(8)−C(13) dihedral angle in the trans CH_3CN complex is calculated to be 90.0°, which is in better agreement with the Pt(AAA)Cl·PPh_3 crystal structure value of 93.3°, although still off by 3.3°. This calculated dihedral angle now puts the benzaldehyde ring at an approximate angle of 90° with respect to the platinum square plane, as compared to 87° for the Pt(AAA)Cl·PPh_3 structure. The increase in the calculated C(7)−N(2)−C(8)−C(13) dihedral angle has also

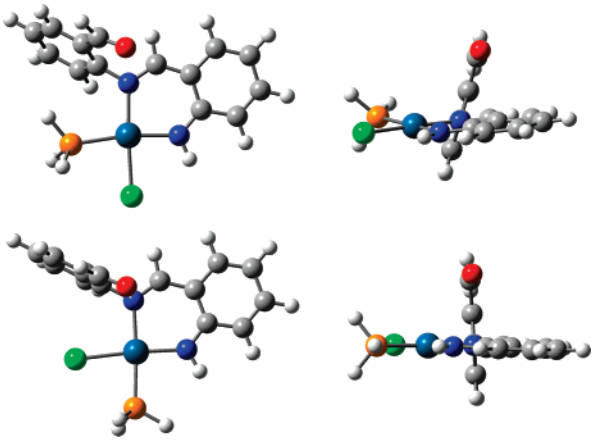

Figure 4. Optimized structure of *cis*-Pt(AAA)Cl·PH_3 (upper) and *trans*-Pt(AAA)Cl·PH_3 (lower) calculated using the B3LYP functional and the 6-31G* basis set on the C, O, N, Cl, H, and P atoms and a modified Hay-Wadt ECP on the Pt atom. The right panel in both the upper and lower is the view along the N(2)−C(8) bond to emphasize the C(7)−N(2)−C(8)−C(13) dihedral angle. The color scheme is the same as that in Figure 2, with the addition that phosphorus is orange.

improved the agreement between the experimental and calculated Pt−O distance, with a deviation of 0.05 Å.

In order to further investigate the relative benzaldehyde dihedral angle for cis versus trans geometries, two more calculations were performed to determine if the identity of the ligand (CH_3CN versus PPh_3) has any effect on the calculated dihedral angle. Due to the computational expense of using the triphenylphosphine ligand itself, calculations were performed on cis and trans configurations of a model compound of Pt(AAA)Cl·PPh_3 in which a PH_3 group was used in place of the triphenylphosphine group, Pt(AAA)Cl·PH_3. The B3LYP/6-31G* optimized geometries for the cis and trans configurations of the Pt(AAA)Cl·PH_3 complexes are shown in Figure 4, and selected values of the bond lengths, bond angles, and dihedral angles are listed in Table 1. Similar to the CH_3CN complexes, the cis and trans PH_3 complexes both reproduce the approximate square planar geometry around the platinum fairly well as compared to the Pt(AAA)Cl·PPh_3 structure. The mean absolute deviation of the bond lengths is found to be 0.03 ± 0.02 Å (4 values) and 0.02 ± 0.03 Å (4 values), respectively, for the cis and trans complexes, and the mean absolute deviation of the bond angles is found to be 1.5 ± 1.8° (2 values) and 2.2 ± 2.1° (4 values), respectively. The most significant difference between the optimized *cis*- and *trans*-Pt(AAA)Cl·PH_3 geometries is with the C(7)−N(2)−C(8)−C(13) dihedral angles, which are 70.1 and 93.6°, respectively. These values deviate from the Pt(AAA)Cl·PPh_3 crystal structure value (93.3°) by 23.2 and 0.3°, respectively. Similar to the calculated dihedral angles for the *cis*- and *trans*-Pt(AAA)-Cl·CH_3CN complexes, the dihedral angle for the cis configuration deviates significantly from that of the Pt(AAA)Cl·PPh_3 crystal structure, while the dihedral angle for the trans configuration is much closer to the experimental value and, in fact, in this case is in excellent agreement with the experimental value.

The results of the cis and trans optimizations with both ligands, when taken together, clearly suggest that the calculated benzaldehyde dihedral angle is affected by two influences, one large and one small. The larger influence is the cis versus trans orientation of the ligand, with the cis orientation resulting in a smaller dihedral angle, presumably due to repulsive steric interactions between the ligand and the benzaldehyde ring. Given the similar dihedral angles for the cis structures of both ligands, the magnitude of this repulsive cis interaction appears to be approximately the same for both ligands, although the smaller PH_3 ligand does seem to have slightly less repulsive interactions since it gives rise to the larger dihedral angle. The smaller, more subtle influence is with the identity of the ligand when it is in the trans orientation, with the PH_3 ligand resulting in a slightly larger dihedral angle. This appears to be a classic "trans effect",[24] in that the nature and bonding strength of the ligand has an effect on the strength and therefore the length of the bond trans to itself, which is the Pt−N(2) bond in these trans complexes. As can be seen from Table 1, the Pt−N(2) bond length is larger in the PH_3 complex (2.08 Å) as compared to the CH_3CN complex (2.03 Å), and this most likely results in slightly smaller repulsive interactions between the benzaldehyde ring and the Cl atom and, therefore, a larger dihedral angle for the PH_3 complex.

Even though optimizations were performed on both cis and trans configurations of the Pt(AAA)Cl·CH_3CN and Pt-(AAA)Cl·PH_3 complexes in order to determine the reason for the large difference between the calculated C(7)−N(2)−C(8)−C(13) dihedral angle for the *cis*-Pt(AAA)Cl·CH_3CN complex and the experimental value for the Pt(AAA)Cl·PPh_3 crystal structure, the discussion of the optimized Pt(AAA)-Cl·CH_3CN transition-state geometry as well as the remaining portions of this paper (vibrational frequencies, excited-state calculations, and reaction energetics) will, in general, only be concerned with the cis configuration. The reasoning for this is 2-fold. The first is that the energy of the *trans*-Pt-(AAA)Cl·CH_3CN complex is found to be approximately 15 kJ/mol higher than that of the *cis*-Pt(AAA)Cl·CH_3CN complex at the B3LYP/6-31G* level, and the second is that there is a large amount of experimental evidence regarding the retention of configuration in square planar substitution reactions,[24,25] of which this reaction could be classified as.

The optimized geometry of the *cis*-Pt(AAA)Cl·CH_3CN transition state is shown in Figure 5, and selected values of the bond lengths, bond angles, and dihedral angles are listed in Table 2. It was verified that this structure was a transition state by a vibrational frequency analysis that indicated one imaginary frequency ($-163\ cm^{-1}$) corresponding primarily to the motion of the benzaldehyde and acetonitrile groups. As can be seen from Figure 5, the transition-state geometry around the platinum is a five-coordinate distorted trigonal bipyramid. The bond lengths of the Pt−Cl, Pt−N(1), and Pt−N(2) bond lengths are similar to those calculated in the Pt(AAA)Cl and *cis*-Pt(AAA)Cl·CH_3CN complexes (Table 1), while the Pt−O and Pt−N_{Ac} distances are significantly larger at 2.57 and 2.49 Å, respectively, which is to be expected since these are the groups undergoing the primary changes in the transition state. In terms of bond angles, the

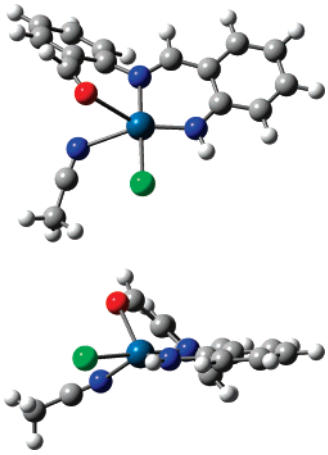

Figure 5. Optimized structure of the *cis*-Pt(AAA)Cl·CH_3CN transition state calculated using the B3LYP functional and the 6-31G* basis set on the C, O, N, Cl, and H atoms and a modified Hay-Wadt ECP on the Pt atom. The view in the lower panel is from the right side of the upper panel. The color scheme is the same as that in Figure 2. Note that the lines drawn between the platinum atom and the benzaldehyde oxygen and between the platinum atom and the acetonitrile nitrogen are not intended to indicate formal bonds but rather to indicate the geometry around the platinum.

Table 2. Selected Bond Lengths (Å), Bond Angles (deg), and Dihedral Angles (deg) for the *cis*-Pt(AAA)Cl·CH_3CN Transition State Optimized Using Density Functional Theory[a]

parameter[b]	value	parameter[b]	value
	Bond Lengths		
Pt−Cl	2.39	Pt−N_{Ac}	2.49
Pt−N(1)	1.96	Pt−O	2.57
Pt−N(2)	2.04		
	Bond Angles		
Cl−Pt−N(1)	86.6	O−Pt−Cl	98.8
N(1)−Pt−N(2)	92.7	N(1)−Pt−O	140.7
N(2)−Pt−N_{Ac}	94.9	N(1)−Pt−N_{Ac}	150.9
N(2)−Pt−O	81.5	O−Pt−N_{Ac}	68.3
N_{Ac}−Pt−Cl	85.8	Pt−N_{Ac}−C_{Ac}	124.6
	Dihedral Angles		
C(6)−C(7)−N(2)−C(8)	173.8	C(7)−N(2)−Pt−N_{Ac}	155.3
C(7)−N(2)−C(8)−C(13)	133.3	C(7)−N(2)−Pt−O	137.6

[a] Calculations performed using the B3LYP functional and the 6-31G* basis set on the C, O, N, Cl, and H atoms and a modified Hay-Wadt ECP on the Pt atom. [b] Numbering scheme corresponds to that shown in Figure 1; N_{Ac} and C_{Ac} refer to the nitrogen and first carbon of the acetonitrile group, respectively.

Cl−Pt−N(1), N(1)−Pt−N(2), N(2)−Pt−N_{Ac}, and N_{Ac}−Pt−Cl angles are fairly similar to those calculated in the Pt(AAA)Cl and *cis*-Pt(AAA)Cl·CH_3CN complexes; however, the angles involving the carbonyl oxygen (N(2)−Pt−O and O−Pt−Cl) are different. Again, this is due to the fact that the benzaldehyde is one of the groups undergoing the primary changes in the transition state. By comparing the C(7)−N(2)−C(8)−C(13) dihedral angles calculated for the Pt(AAA)Cl and *cis*-Pt(AAA)Cl·CH_3CN complexes with that of the transition state, one can also see that the transition-state dihedral angle is intermediate to that of the Pt(AAA)-Cl and *cis*-Pt(AAA)Cl·CH_3CN complexes, which is again as expected. As mentioned above, the overall structure about the platinum is described as a distorted trigonal bipyramid, mostly because of the enlarged N(1)−Pt−O and N(1)−Pt−N_{Ac} angles at 140.7° and 150.9°, respectively, and the squeezed O−Pt−N_{Ac} angle at 68.3°. It is also interesting to note that the acetonitrile group is considerablely off-axis in terms of its approach to the platinum, as judged by the low Pt−N_{Ac}−C_{Ac} angle; however, it is unclear what the cause of this is.

Table 3. Calculated and Experimental Benzaldehyde C═O Vibrational Frequencies (cm^{-1}) for Pt(AAA)Cl, the *cis*-Pt(AAA)Cl·CH_3CN Transition State, and *cis*-Pt(AAA)Cl·CH_3CN[a]

species	HF/ STO-3G	HF/ 3-21G	HF/ 6-31G*	B3LYP/ 6-31G*	expt
Pt(AAA)Cl	1968	1814	1919	1656	1621[b]
Pt(AAA)Cl·CH_3CN transition state	2028	1876	1994	1765	
Pt(AAA)Cl·CH_3CN	2039	1912	2014	1805	1690[c]

[a] The theoretical method and the basis set used for the C, O, N, Cl, and H atoms is indicated in the column headings; a modified Hay-Wadt ECP was used on the Pt atom for all calculations. [b] Reference 6. [c] Reference 7.

Calculated C═O Vibrational Frequencies. Vibrational analysis was performed for the optimized structures of the Pt(AAA)Cl and *cis*-Pt(AAA)Cl·CH_3CN complexes as well as the *cis*-Pt(AAA)Cl·CH_3CN transition state at several levels of theory, and the calculated frequencies for the benzaldehyde C═O stretching modes are listed in Table 3. Experimental vibrational frequencies for the benzaldehyde C═O stretching mode of the Pt(AAA)Cl and Pt(AAA)Cl·CH_3CN complexes are also listed in Table 3.[6,7] As can be seen in Table 3, the C═O stretching frequency is predicted to increase on going from being fully coordinated in the Pt(AAA)Cl complex, partially coordinated in the *cis*-Pt(AAA)Cl·CH_3CN transition state, and uncoordinated in *cis*-Pt(AAA)Cl·CH_3CN complex at each level of theory examined. These results are in qualitative agreement with the experimentally observed behavior for the Pt(AAA)Cl and *cis*-Pt(AAA)Cl·CH_3CN complexes, and the calculated frequencies lend support to the experimental assignments. A decrease in the C═O frequency upon complexation has also been experimentally observed with other metal complexes of ketones and aldehydes.[26]

Since the experimental C═O stretching frequencies have been reported for the Pt(AAA)Cl and Pt(AAA)Cl·CH_3CN complexes, a quantitative comparison can be made with the theoretically calculated values. At all of the levels of theory examined, the theoretical C═O stretching frequencies are predicted to be larger than the experimental values, which is typical and due to known systematic factors such as neglect of anharmonicity, complete or incomplete neglect of electron correlation, and the use of finite basis sets.[11,27] The magnitude of the deviations are found to change with the method and the basis set, with the largest average deviation being at the HF/STO-3G level (∼17.4%) and the smallest average

deviation being at the B3LYP/6-31G* level (~4.2%), consistent with both an increase in the size of the basis set and the inclusion of electron correlation.[11,27,28] There does, however, appear to be a discontinuity in the deviations, with the average deviation at the HF/3-21G level (~11.1%) being lower than the average deviation at the HF/6-31G* level (~15.8%). This seemingly anomalous trend has been observed and reported previously in a systematic study comparing the theoretical versus experimental vibrational frequencies of over 1000 molecules at various levels of theory.[28] In this study, it was found that the average deviation at the HF/3-21G level was approximately 9.2%, and at the HF/6-31G* level the average deviation was 10.5%.

In addition to comparing the absolute magnitudes of the experimental and calculated C═O stretching frequencies for the Pt(AAA)Cl and *cis*-Pt(AAA)Cl·CH_3CN complexes, it is also of interest to quantitatively compare the experimental versus the theoretical shift in this frequency between the two complexes. As shown in Table 3, the experimental C═O stretching frequencies for the Pt(AAA)Cl and Pt(AAA)Cl·CH_3CN complexes were determined to be 1621 and 1690 cm^{-1}, respectively, corresponding to a shift of 69 cm^{-1}. The theoretical shift for this vibrational mode in the two complexes is predicted to be 71, 98, 95, and 149 cm^{-1} at the HF/STO-3G, HF/3-21G, HF/6-31G*, and B3LYP/6-31G* levels, respectively. Overall, the magnitudes of the predicted shifts are in reasonable agreement with the experimentally observed value, again lending support to the experimental assignment of these bands to the C═O stretching vibrations in the two complexes. It is worth noting that the best agreement appears to be at the HF/STO-3G level; however, this is most likely fortuitous.

Singlet Excitation Energies. Singlet vertical excitation energies were calculated for the B3LYP/6-31G* optimized Pt(AAA)Cl and *cis*-Pt(AAA)Cl·CH_3CN geometries using time-dependent density-functional theory (TDDFT) with the B3LYP hybrid functional and the 6-31+G*, 6-311+G*, and the 6-311+G(2d,2p) basis sets. The calculated excitation energies, transition wavelengths, and oscillator strengths for the first three excited states of the Pt(AAA)Cl and *cis*-Pt(AAA)Cl·CH_3CN complexes are listed in Table 4. As can be seen from Table 4, the Pt(AAA)Cl and *cis*-Pt(AAA)Cl·CH_3CN energies calculated for a given transition using the three different basis sets are very close to one another, with deviations between 0.02 and 0.04 eV, which suggests that basis set size does not have a large effect on the calculated excitation energies. However, it is worth noting that the transition energies do display a subtle basis set effect, in that a small decrease in the state energy is generally observed with an increasing basis set size. For simplicity in the following discussion, generally only the excited-state results using the largest basis set, 6-311+G(2d,2p), will be described in detail below.

For the Pt(AAA)Cl complex, the calculations predict the transition to the S_1 state to be the most intense of the first three excited states ($f = 0.130$), with a transition energy of 2.18 eV and a transition wavelength of 568 nm. The dominant orbital excitation for the S_1 state is the HOMO to LUMO transition, and both of these orbitals, calculated at the B3LYP/6-311+G(2d,2p) level, are displayed in Figure 6. As can be seen from Figure 6, both of these orbitals are primarily admixtures of Pt d orbitals and π orbitals on the AAA ligand. The most significant difference between them is that the HOMO orbital has significant Cl p orbital character, while the LUMO has zero Cl orbital character. Therefore, this transition can at least partially be classified as a Cl-to-Pt/AAA charge-transfer transition. The transitions

Table 4. Low-Lying Singlet Excited States for Pt(AAA)Cl and for *cis*- and *trans*-Pt(AAA)Cl·CH_3CN Calculated with Time-Dependent Density Functional Theory Using the B3LYP Functional (Unless Noted) and Various Basis Sets[a]

	6-31+G*			6-311+G*			6-311+G(2d,2p)		
state	E^b (eV)	λ^c (nm)	f^d	E^b (eV)	λ^c (nm)	f^d	E^b (eV)	λ^c (nm)	f^d
				Pt(AAA)Cl					
S_1	2.21	560	0.137	2.20	565	0.131	2.18	568	0.130
S_2	2.56	483	0.033	2.54	487	0.037	2.53	490	0.037
S_3	2.68	463	0.016	2.66	466	0.015	2.64	469	0.015
S_1[e]	2.22	559	0.133						
S_2[e]	2.57	482	0.038						
S_3[e]	2.69	461	0.015						
				cis-Pt(AAA)Cl·CH_3CN					
S_1	2.07	600	0.017	2.06	601	0.017	2.05	604	0.017
S_2	2.85	435	0.047	2.84	437	0.047	2.82	440	0.047
S_3	2.91	426	0.006	2.91	426	0.005	2.93	423	0.004
S_1[e]	2.08	595	0.017						
S_2[e]	2.86	433	0.048						
S_3[e]	2.92	424	0.004						
				trans Pt(AAA)Cl·CH_3CN					
S_1	2.49	498	0.000						
S_2	2.83	437	0.046						
S_3	3.03	409	0.000						

[a] The basis set used for the C, O, N, Cl, and H atoms is indicated in the column headings; a modified Hay-Wadt ECP was used on the Pt atom for all calculations. [b] Calculated transition energy. [c] Calculated transition wavelength. [d] Calculated oscillator strength. [e] Calculated using the B3PW91 functional.

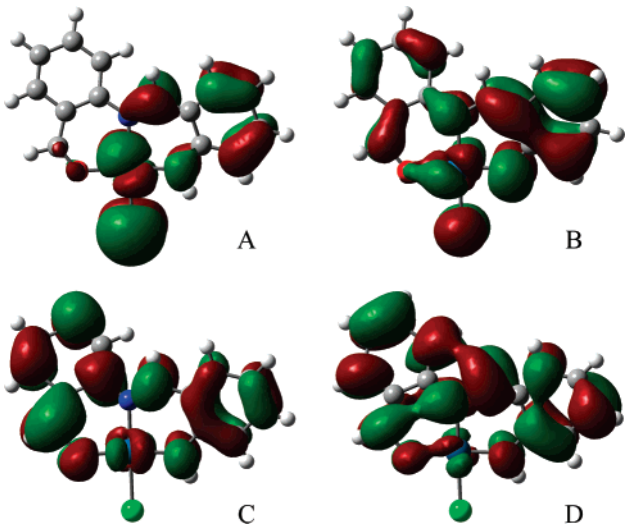

Figure 6. Contour plots of the (a) HOMO − 1, (b) HOMO, (c) LUMO, and (d) LUMO + 1 molecular orbitals of Pt(AAA)Cl calculated using the B3LYP functional and the 6-311+G(2d,2p) basis set on the C, O, N, Cl, and H atoms and a modified Hay-Wadt ECP on the Pt atom.

to the S_2 and S_3 states are predicted to have energies of 2.53 and 2.64 eV, respectively, corresponding to wavelengths of 490 and 469 nm, respectively; however, their intensities are reduced by a factor of 3.5 ($f = 0.037$) and 8.7 ($f = 0.015$), respectively, as compared to the S_1 state. The dominant orbital excitations for the S_2 and S_3 states are the HOMO − 1 to LUMO and HOMO to LUMO + 1 transitions, respectively. The HOMO − 1 and LUMO + 1 orbitals, calculated at the B3LYP/6-311+G(2d,2p) level, are also displayed in Figure 6. The HOMO − 1 orbital is also primarily an admixture of a Pt d orbital, a Cl p orbital, and a π orbital on the AAA ligand; however, in this case the AAA ligand π orbital is almost exclusively centered on the o-aminobenzylidene (OAB) portion of the ring. Comparing the HOMO − 1 to the LUMO orbital, the S_2 transition can be classified as a combination of a Cl-to-Pt/AAA charge-transfer transition and an AAA intraligand charge-transfer transition (OAB ring to the benzaldehyde ring). Similar to the LUMO orbital, the LUMO + 1 orbital is an admixture of a Pt d orbital and a π orbital on the entire AAA ligand, with zero Cl orbital character. Comparing the HOMO to the LUMO + 1 orbital, the S_3 transition can be classified as a Cl-to-Pt/AAA charge-transfer transition.

Experimentally the visible absorption spectrum of the Pt(AAA)Cl complex has been reported by Mertes and co-workers in $CHCl_3$ and acetonitrile[6,7] and consists of a moderately intense, broad band centered at 578 ($\epsilon = 1.4 \times 10^4$ M^{-1} cm^{-1}) and 560 nm ($\epsilon = 1.0 \times 10^4$ M^{-1} cm^{-1}), respectively, which correspond to experimental transition energies of 2.14 and 2.21 eV, respectively. Comparing the experimental energies to the calculated energy for the S_1 state, it is found that the calculated energy of the S_1 state is in very good agreement with the two experimental values, with deviations of 0.04 and 0.03 eV, respectively.

Upon cis complexation of the CH_3CN, the calculations predict that the energy of the transition to the S_1 state is red-shifted compared to Pt(AAA)Cl, with a value of 2.05 eV (604 nm) and that its intensity is reduced by a factor of 7.6 ($f = 0.017$) as compared to Pt(AAA)Cl. The dominant orbital excitation for the S_1 state of *cis*-Pt(AAA)Cl·CH_3CN is the HOMO to LUMO transition, and both of these orbitals, calculated at the B3LYP/6-311+G(2d,2p) level, are displayed in Figure 7. As can be seen in Figure 7, the HOMO orbital is primarily an admixture of a Pt d orbital, a Cl p orbital, and a π orbital localized on the OAB portion of the AAA ligand. The LUMO orbital, on the other hand, is primarily a π orbital localized on the benzaldehyde portion of the AAA ligand, with small contributions from the Pt and Cl atoms. This transition can then be classified as a Pt/Cl/OAB-to-benzaldehyde charge-transfer type transition. The energies of the S_2 and S_3 states of the *cis*-Pt(AAA)Cl·CH_3CN complex are predicted to be blue-shifted with respect to those of Pt(AAA)Cl, with energies of 2.82 and 2.93 eV, respectively. The intensities of the transitions to the S_2 and S_3 states are predicted to increase by a factor of 1.3 ($f = 0.047$) and decrease by a factor of 3.8 ($f = 0.004$), respectively, relative to the intensities of these transitions for Pt(AAA)Cl. The dominant orbital excitations for the S_2 and S_3 states are the HOMO to LUMO + 1 and the HOMO to LUMO + 2 transitions, respectively, and the LUMO + 1 and LUMO + 2 orbitals calculated at the B3LYP/6-311+G(2d,2p) level are displayed in Figure 7. The LUMO + 1 orbital is primarily an admixture of a Pt d orbital and a π orbital that is delocalized over most of the AAA ligand and has zero Cl orbital character. Comparing the HOMO to the LUMO + 1 orbital, the S_2 transition can be classified as a combination of a Cl-to-Pt/AAA charge-transfer transition and an AAA intraligand charge-transfer transition (OAB ring to the benzaldehyde ring). The LUMO + 2 orbital is an admixture of a Pt d orbital, a Cl p orbital, and a fairly delocalized AAA π orbital. Comparing the HOMO to the LUMO + 2 orbital, the S_3 transition can be classified as a Cl/Pt/OAB-to-benzaldehyde charge-transfer transition.

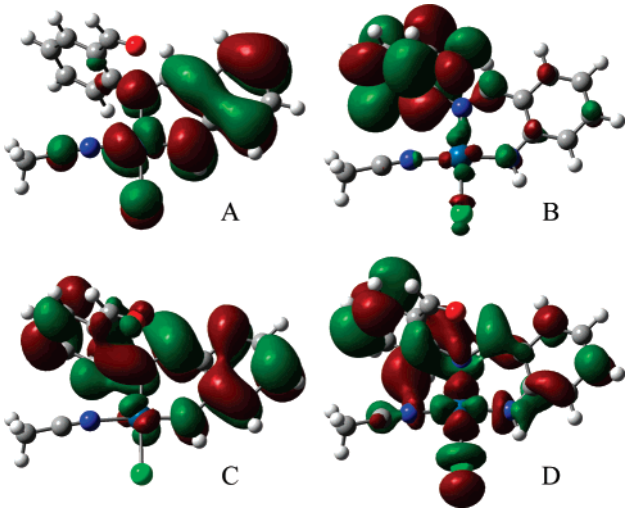

Figure 7. Contour plots of the (a) HOMO, (b) LUMO, (c) LUMO + 1, and (d) LUMO + 2 molecular orbitals of *cis*-Pt(AAA)Cl·CH_3CN calculated using the B3LYP functional and the 6-311+G(2d,2p) basis set on the C, O, N, Cl, and H atoms and a modified Hay-Wadt ECP on the Pt atom.

Experimentally the absorption spectrum of the Pt(AAA)Cl·CH_3CN complex in the visible region has been reported by Mertes and co-workers in acetonitrile[7] and is comprised of a low intensity, broad band centered at 470 nm ($\epsilon = 4.0 \times 10^3$ M^{-1} cm^{-1}), which corresponds to an energy of 2.64 eV. Upon initial comparison of the energy of the experimentally reported λ_{max} and the energy of the calculated S_1 transition, it appears as if there is a large discrepancy of 0.59 eV. Given the good agreement between the calculated and experimental transition of the Pt(AAA)Cl complex, however, this was very surprising and seemed unlikely. Upon closer inspection of the published spectrum assigned to the Pt(AAA)Cl·CH_3CN complex by Mertes and co-workers, it is observed that the most intense feature in the visible region is indeed the band centered at 470 nm; however, there still remains a broad, low intensity ($\epsilon \approx 1.0 \times 10^3$ M^{-1} cm^{-1}) band between 550 and 600 nm in the spectrum. Since the calculated relative intensities of the S_1 and S_2 transitions for the *cis*-Pt(AAA)Cl·CH_3CN complex are similar to the experimental molar absorptivities of the 470 nm band and the region between 550 and 600 nm, this suggests that the energy of the 470 nm band (2.64 eV) should be quantitatively

Table 5. Zero-Point Corrected Total Energies, Enthalpies, Entropies, and Free Energies at 298 K for CH_3CN, Pt(AAA)Cl, *cis*-Pt(AAA)Cl·CH_3CN, and the *cis*-Pt(AAA)Cl·CH_3CN Transition State Calculated at the B3LYP/6-311+G(2d,2p) Level[a]

species	E^{298} (hartrees)	H^{298} (hartrees)	S^{298} (J/K·mol)	G^{298} (hartrees)
CH_3CN	−132.751806	−132.750862	242.6	−132.778421
Pt(AAA)Cl	−1304.292137	−1304.291193	539.8	−1304.352518
cis-Pt(AAA)Cl·CH_3CN	−1437.046106	−1437.045161	684.7	−1437.122948
Pt(AAA)Cl·CH_3CN TS[b]	−1437.014532	−1437.013588	660.0	−1437.088560

[a] Calculations performed using the 6-311+G(2d,2p) basis set on the C, O, N, Cl, and H atoms and a modified Hay-Wadt ECP on the Pt atom. [b] *cis*-Pt(AAA)Cl·CH_3CN transition state.

compared to the calculated energy of the S_2 transition (2.82 eV). With this comparison, the agreement now seems reasonable, with a deviation of 0.18 eV. Another factor that supports this assignment is the good agreement of the relative molar absorptivities of the 560 nm band of Pt(AAA)Cl ($\epsilon = 1.0 \times 10^4$ M^{-1} cm^{-1}) to the 470 nm band of Pt(AAA)Cl·CH_3CN ($\epsilon = 4.0 \times 10^3$ M^{-1} cm^{-1}) with the relative calculated oscillator strengths of the S_1 transition of Pt(AAA)Cl ($f = 0.130$) to the S_2 transition of *cis*-Pt(AAA)Cl·CH_3CN ($f = 0.047$).

In order to further assess the validity of the calculated transitions for the *cis*-Pt(AAA)Cl·CH_3CN complex and the assignments made above, several other TDDFT excited-state calculations were performed. These additional TDDFT calculations were Pt(AAA)Cl and *cis*-Pt(AAA)Cl·CH_3CN at the B3PW91/6-31+G* level and *trans*-Pt(AAA)Cl·CH_3CN at the B3LYP/6-31+G* level, the results of which are given in Table 4. Comparing the results for Pt(AAA)Cl and *cis*-Pt(AAA)Cl·CH_3CN at the B3PW91/6-31+G* level to those at the B3LYP/6-31+G* level, it is clear that the B3PW91 functional predicts nearly the same transition energies and oscillator strengths for the Pt(AAA)Cl and *cis*-Pt(AAA)Cl·CH_3CN complexes as the B3LYP calculations, supporting the validity of the B3LYP calculations. With the *trans*-Pt(AAA)Cl·CH_3CN complex at the B3LYP/6-31+G* level, the calculations predict the S_1 transition to be at a higher energy than for the *cis*-Pt(AAA)Cl·CH_3CN complex; however, the oscillator strength is predicted to be zero. The calculated energy and oscillator strength for the S_2 transition of the *trans*-Pt(AAA)Cl·CH_3CN complex, in contrast, are very close to the values for the S_2 transition of the *cis*-Pt(AAA)Cl·CH_3CN complex. Similar to the S_1 transition, the energy of the S_3 transition is predicted to be higher for the *trans*-Pt(AAA)Cl·CH_3CN complex than it is for the *cis*-Pt(AAA)Cl·CH_3CN complex, and the oscillator strength is calculated to be zero for the trans complex. Overall, the additional calculations support the hypothesis that once the CH_3CN is bound to the platinum, the S_2 transition becomes the most intense transition in the visible region and that it is blue-shifted and its intensity is decreased when compared to the most intense, S_1 transition for Pt(AAA)Cl.

Dark Reaction Thermochemistry and Activation Parameters. Single point energies were calculated at the B3LYP/6-311+G(2d,2p) level using the B3LYP/6-31G* optimized geometries for CH_3CN, the Pt(AAA)Cl complex, the *cis*-Pt(AAA)Cl·CH_3CN complex, and the *cis*-Pt(AAA)Cl·CH_3CN transition state. Using the scaled (0.9804[22]) B3LYP/6-31G* vibrational frequencies, zero-point and 298 K thermal corrections were determined, allowing for the calculation of 0 K energies and 298 K enthalpies, entropies, and free energies, which are listed in Table 5.

Utilizing the parameters for CH_3CN, Pt(AAA)Cl, and *cis*-Pt(AAA)Cl·CH_3CN in Table 5, the thermochemistry of the dark reaction, Pt(AAA)Cl + $CH_3CN \rightarrow$ Pt(AAA)Cl·CH_3CN, can be calculated. The 298 K reaction energy and reaction enthalpy are both calculated to be exothermic, with values of −5.7 and −8.2 kJ/mol, respectively, indicating that the dark reaction is slightly energetically favorable. The 298 K entropy change for the dark reaction is found to be negative, which is consistent with two molecules going to one molecule, and has a calculated value of −97.7 J/K·mol using the absolute entropies in Table 5. Somewhat surprisingly, since the reaction is experimentally known to occur spontaneously in solution,[7] the 298 K free energy of the dark reaction is predicted to be endergonic in the gas phase, with a value of +21.0 kJ/mol. The primary reason for the large positive calculated ΔG^{298} is due to the large negative entropy, which causes the magnitude of $T\Delta S^{298}$ to be larger than the ΔH^{298}. Experimentally, this reaction occurs in acetonitrile as the solvent, and, in order to calculate an approximate free energy for the reaction in the condensed phase, the liquid-phase absolute entropy of acetonitrile (149.6 J/K·mol[29]) can be used in the calculation of $\Delta S^{298.}$ Using the liquid-phase entropy for acetonitrile, the condensed-phase values of ΔS^{298} and ΔG^{298} are calculated to be −4.7 J/K·mol and −6.7 kJ/mol, respectively, and the reaction is now predicted to be spontaneous, as it is experimentally known to be. This seems to be an example of a reaction in which solvent/condensed-phase considerations have a large effect on the spontaneity of the reaction. Unfortunately, no experimental thermochemical parameters have been reported for the dark reaction of this complex, and so a comparison to experimental values is not possible. However, the thermochemistry of ligand substitution reactions for several square planar Pt(II) complexes has been studied both experimentally[30] and theoretically,[31] and the current values are found to be within the range of values reported previously.

Since single point and frequency calculations been performed on the *cis*-Pt(AAA)Cl·CH_3CN transition state, the activation parameters of the dark reaction can also be calculated using the values for CH_3CN, Pt(AAA)Cl, and the *cis*-Pt(AAA)Cl·CH_3CN transition state (Table 5). The 298 K activation energy is calculated to be 77.2 kJ/mol, and the 298 K activation enthalpy is calculated to be 74.7 kJ/mol. The gas-phase activation entropy and free energy are calculated to be −122.5 J/k·mol and 111.2 kJ/mol, respectively. However, in light of the discussion above concerning the condensed-phase reaction entropy and free energy,

condensed-phase values are also calculated using the liquid-phase absolute entropy of acetonitrile and are found to be −29.5 J/k·mol and 83.5 kJ/mol for the condensed-phase activation entropy and the activation free energy, respectively. Unfortunately, experimental values of the activation energy and the activation enthalpy for the dark reaction of Pt(AAA)Cl have not been reported in the literature, and so a direct comparison to the calculated values is not possible. However, activation enthalpies have been measured for nucleophilic substitution reactions of several platinum(II) complexes, and these are found to vary from approximately 30−100 kJ/mol.[24] In light of these values, the calculated activation enthalpy for the dark reaction seems reasonable.

Energetics and Mechanism of the Photoreaction. In addition to the energetics of the dark reaction, it also of interest to attempt to characterize the energetics and mechanism of the photoreaction. In general, there are two typical mechanisms for photochemical or photoinduced reactions: adiabatic and diabatic reactions. In an adiabatic photoreaction, the reactants are excited and then traverse along the excited-state surface over an excited-state activation barrier to the excited state of the products. The ground-state products are then reached via radiative or nonradiative decay. In the diabatic reaction, the reactants are excited and traverse along the excited-state surface to a point at which the excited-state and ground-state surfaces closely approach one another, usually close to where the ground state is a maximum, i.e., the ground transition state.[32] This is then followed by a surface crossing from the excited-state surface to the ground-state surface and finally ground-state relaxation down to the products or back to the ground state of the reactants, in which case no overall reaction has occurred. Because the present reaction involves platinum(II) complexes and it has been long known that platinum(II) complexes often display very strong phosphorescence emission even at room temperature[33−38] and therefore have very large singlet to triplet intersystem crossing rates, the possibility that the photoreaction occurs via the lowest triplet-state surface needs to be also considered.

In order to determine along which surface the reaction proceeds and which of the two mechanisms is most probable, the location of the Pt(AAA)Cl and *cis*-Pt(AAA)Cl·CH_3CN minima and the *cis*-Pt(AAA)Cl·CH_3CN transition-state maxima along the S_1 and T_1 potential energy surfaces would be needed, which would require S_1 and T_1 geometry optimizations. Unfortunately, geometry optimizations coupled with TDDFT calculations are not currently available in the Gaussian suite of programs. However, using calculated S_1 and T_1 vertical excitations for the ground-state optimized Pt(AAA)Cl, *cis*-Pt(AAA)Cl·CH_3CN, and *cis*-Pt(AAA)Cl·CH_3CN transition state, some indications of the energetics and the most likely mechanism for the photoreaction can be inferred.

For consistency in comparison with the highest level ground-state energetics, only vertical excitation energies calculated at the B3LYP/6-311+G(2d,2p) level will be used in this discussion. For Pt(AAA)Cl and *cis*-Pt(AAA)Cl·CH_3CN, the S_1 excitation energies are taken from Table 4 and converted to kJ/mol, giving 210 and 198 kJ/mol, respectively. The S_1 vertical excitation energy for the *cis*-Pt(AAA)Cl·CH_3CN transition state was calculated to be 1.80 eV or 173 kJ/mol at the B3LYP/6-311+G(2d,2p) level. The T_1 vertical excitation energies for Pt(AAA)Cl, *cis*-Pt(AAA)Cl·CH_3CN, and the *cis*-Pt(AAA)Cl·CH_3CN transition state were calculated to be 1.42, 1.84, and 1.37 eV, respectively, at the B3LYP/6-311+G(2d,2p) level, which correspond to 137, 178, and 132 kJ/mol, respectively. By combining the S_1 and T_1 vertical excitation energies with the ground-state (S_0) energies of these species relative to the Pt(AAA)Cl and CH_3CN reactants, the relative energetics of these species along the S_1 and T_1 potential energy surfaces can be obtained, and these are represented in Figure 8.

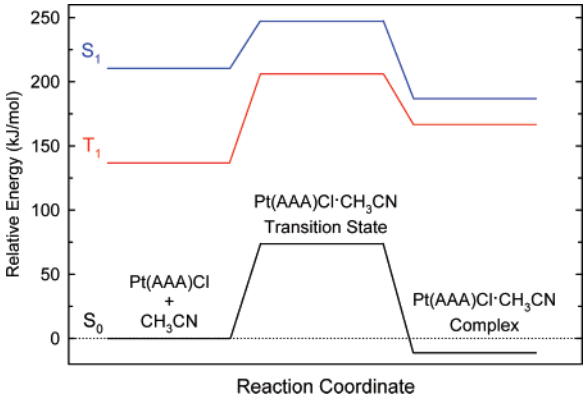

Figure 8. Relative energy diagram for the S_0, S_1, and T_1 states of the Pt(AAA)Cl + CH_3CN reactants, the *cis*-Pt(AAA)Cl·CH_3CN transition state, and the *cis*-Pt(AAA)Cl·CH_3CN complex calculated using the B3LYP functional and the 6-311+G(2d,2p) basis set on the C, O, N, Cl, and H atoms and a modified Hay-Wadt ECP on the Pt atom.

From Figure 8, it can be seen that the reaction from *cis*-Pt(AAA)Cl·CH_3CN to Pt(AAA)Cl along the S_1 surface is predicted to be endothermic by 24 kJ/mol and to have an energy barrier of 62 kJ/mol. In contrast to the S_1 surface, the same reaction along the T_1 surface is predicted to be exothermic by 29 kJ/mol and to have an energy barrier of 42 kJ/mol. The S_1-T_1 energy gap for *cis*-Pt(AAA)Cl·CH_3CN is predicted to be 20.1 kJ/mol, which seems small enough that S_1 to T_1 intersystem crossing would probably occur with an appreciable rate. Therefore, based on these relative energies, it seems likely that upon absorption of a photon to reach the S_1 state or absorption to S_2 followed by fast internal conversion to S_1, rapid intersystem crossing to T_1 occurs, and the photoreaction then proceeds along the T_1 surface. The last question to address is whether the photoreaction follows an adiabatic mechanism along the T_1 surface or a diabatic mechanism involving a crossing from the T_1 surface to a maximum along the S_0 surface. Because the T_1 excitations for each of the molecules along the reaction involve fairly delocalized HOMO and LUMO orbitals (see Figures 6 and 7 for example) and are therefore not expected to cause very large changes in the bonding upon excitation, it seems reasonable to assume that the geometries of the minima and maxima along the T_1 surface would be similar to those along S_0. This then implies that a diabatic mechanism involving a surface crossing from a low-energy point along T_1 to a high-energy point along S_0 is unlikely and that the photoreaction proceeds adiabatically along T_1 from *cis*-Pt-

(AAA)Cl·CH_3CN over the T_1 energy barrier to the T_1 state of Pt(AAA)Cl. The final step in the photoreaction, which is the relaxation from the T_1 state to the S_0 state of Pt(AAA)Cl, most likely occurs via nonradiative intersystem crossing, given that Mertes and co-workers[7] did not report observing the re-emission of light for the photoreaction of Pt(AAA)Cl·CH_3CN back to Pt(AAA)Cl.

Summary and Conclusion

Density functional theory methods have been used to theoretically characterize a tridentate photochromic Pt(II) complex [Pt(AAA)Cl], its acetonitrile solvolyis product [Pt(AAA)Cl·CH_3CN], and the transition state in the solvolysis reaction. The geometries were optimized at the B3LYP/6-31G* level of theory. The optimized geometry of Pt(AAA)Cl was found to be in good agreement with the reported crystal structure.[6] The optimized geometry of *cis*-Pt(AAA)Cl·CH_3CN was also found to be in good agreement with most of the applicable geometrical parameters for a crystal structure reported for a related complex with triphenylphosphine as the ligand, *trans*-Pt(AAA)Cl·PPh_3,[10] the exception being the C(7)−N(2)−C(8)−C(13) dihedral angle. Additional optimizations were performed for *trans*-Pt(AAA)Cl·CH_3CN and for *cis*- and *trans*-Pt(AAA)Cl·PH_3. As a result, it was found that the deviation in the dihedral angle between the calculated *cis*-Pt(AAA)Cl·CH_3CN value and the experimental *trans*-Pt(AAA)Cl·PPh_3 value was primarily due to a steric cis versus trans effect. Vibrational frequencies were calculated for the optimized Pt(AAA)Cl and *cis*-Pt(AAA)Cl·CH_3CN complexes at several levels of theory, and it was found that the predicted shift in the benzaldehyde carbonyl frequency for Pt(AAA)Cl to *cis*-Pt(AAA)Cl·CH_3CN was in the same direction and close to that observed experimentally,[6,7] supporting the experimental assignments. Singlet vertical excitation energies were calculated for the B3LYP/6-31G* optimized Pt(AAA)Cl and *cis*-Pt(AAA)Cl·CH_3CN geometries using time-dependent density-functional theory (TDDFT). The most intense transition for Pt(AAA)Cl was predicted to be to the S_1 state, and its energy was found to be in good agreement with the experimental value. The most intense transition for *cis*-Pt(AAA)Cl·CH_3CN, however, was predicted to be to the S_2 state rather than to the S_1 state, and the energy of this transition was found to be in reasonable agreement with the experimental value. Overall, the excited-state calculations support the experimental observation of a blue-shift and a decrease in intensity on going from Pt(AAA)Cl to *cis*-Pt(AAA)Cl·CH_3CN. Single point energies were calculated at the B3LYP/6-311+G(2d,2p) level using the B3LYP/6-31G* optimized geometries for CH_3CN, the Pt(AAA)Cl complex, the *cis*-Pt(AAA)Cl·CH_3CN complex, and the *cis*-Pt(AAA)Cl·CH_3CN transition state. The calculations predict the dark reaction to be slightly exothermic at 298 K and, after a correction to the entropy, to also be spontaneous at 298 K, and to proceed with a reasonable activation energy. For the photoreaction, approximate excited-state energies were obtained using the vertical S_1 and T_1 energies for *cis*-Pt(AAA)Cl·CH_3CN, the *cis*-Pt(AAA)Cl·CH_3CN transition state, and Pt(AAA)Cl, and based on these energies relative to the ground-state energies, it was speculated that the photoreaction occurs via an intersystem crossing from S_1 to T_1 for *cis*-Pt(AAA)Cl·CH_3CN followed by an adiabatic reaction along the T_1 surface to the T_1 state of Pt(AAA)Cl and then nonradiative intersystem crossing to the S_0 state of Pt(AAA)Cl.

Acknowledgment. This work was supported by startup funds from Penn State Erie, The Behrend College. I thank Alan Jircitano and Tom Spudich for providing the initial motivation to engage in these calculations and for enlightening discussions during the course of this work. I additionally thank Alan Jircitano for supplying the initial ChemDraw structure that was used for Figure 1. I thank Peter B. Armentrout for providing a Gaussian input file containing the parameters of the modified Hay-Wadt ECP/valence that was used for the Pt in the present work.

Supporting Information Available: Gaussian input with route line, title, Cartesian coordinates, and Pt ECP/valence basis set parameters for all of the optimized geometries obtained in this work. This material is available free of charge via the Internet at http://pubs.acs.org.

References

(1) VerHoeven, J. W. *Pure Appl. Chem.* **1996**, *68*, 2223−2286.

(2) See the following general photochromism references. (a) *Organic Photochromic and Thermochromic Compounds*; Crano, J. C., Guglielmetti, R. J., Eds.; Plenum: New York, 1999; Vols. 1 and 2. (b) *Photochromism: Molecules and Systems*; Durr, H., Bouas-Laurent, H., Eds.; Elsevier: New York 1990; pp 1−1068. (c) See the following issue of *Chem. Rev.*: *Chem. Rev.* **2000**, *100* (5), 1683−1890. (d) See sections I and II of Exelby, R.; Grinter, R. *Chem. Rev.* **1965**, *65*, 247−260.

(3) See the following general reviews of photochromic inorganic compounds. (a) Faughan, B. W.; Staebler, D. L.; Zoltan, K. J. *Appl. Solid State Phys.* **1971**, *2*, 107−172. (b) Zoltan, K. J. *Physics Today* **1970**, *23*, 42−49. (c) Cohen, S. D.; Newman, G. A. *J. Photogr. Sci.* **1967**, *15*, 290−298. (d) See section III of Exelby, R.; Grinter, R. *Chem. Rev.* **1965**, *65*, 247−260.

(4) Particular sections of the following reviews of photochemistry of transition-metal compounds deal with photochromic transition-metal compounds. (a) Adamson, A. W. *Pure Appl. Chem.* **1969**, *20*, 25−52. (b) Adamson, A. W.; Waltz, W. L.; Zinato, E.; Watts, D. W.; Fleischauer, P. D.; D., L. R. *Chem. Rev.* **1968**, *68*, 541−585.

(5) See the following articles and references therein for recent examples of photochromic transition-metal compounds. (a) Miyamoto, Y.; Kikuchi, A.; Iwahori, F.; Abe, J. *J. Phys. Chem. A* **2005**, *109*, 10183−10188. (b) Matsuda, K.; Takayama, K.; Irie, M. *Inorg. Chem.* **2004**, *43*, 482−489. (c) Nishimura, H.; Matsushita, N. *Chem. Lett.* **2002**, *9*, 930−931. (d) Wakamatsu, K.; Nishimoto, K.; Shibahara, T. *Inorg. Chim. Acta* **1999**, *295*, 180−188.

(6) Timken, M. D.; Sheldon, R. I.; Rohly, W. G.; Mertes, K. B. *J. Am. Chem. Soc.* **1980**, *102*, 4716−4720.

(7) Rohly, W. G.; Mertes, K. B. *J. Am. Chem. Soc.* **1980**, *102*, 7939−7942.

(8) For examples, see the following and references therein. (a) Lutterman, D. A.; Fu, P. K.-L.; Turro, C. *J. Am. Chem. Soc.* **2006**, *128*, 738−739. (b) Martinez, M. S.; de Oliveira, E.

C.; Tfouni, E. *J. Photochem. Photobiol., A* **1999**, *122*, 103−108. (c) Kirk, A. D. *Comments Inorg. Chem.* **1993**, *14*, 89−121. (d) Moensted, L.; Moensted, O. *Acta Chem. Scand.* **1993**, *47*, 9−17. (e) Carlos, R. M.; Frink, M. E.; Tfouni, E.; Ford, P. C. *Inorg. Chim. Acta* **1992**, *193*, 159−165. (f) Pavanin, L. A.; Novais, da Rocha, Z.; Giesbrecht, E.; Tfouni, E. *Inorg. Chem.* **1991**, *30*, 2185−2190.

(9) Jircitano, A. J. Penn State Erie, The Behrend College, Erie, PA. Personal communication 2006.

(10) Jircitano, A. J.; Rohly, W. G.; Mertes, K. B. *J. Am. Chem. Soc.* **1981**, *103*, 4879−4883.

(11) Hehre, W. J.; Radom, L.; Schleyer, P. V. R.; Pople, J. A. *Ab Initio Molecular Orbital Theory*; Wiley & Sons: New York, 1986; pp 1−548.

(12) Ziegler, T. *Chem. Rev.* **1991**, *91*, 651−667.

(13) Koch, W.; Holthausen, M. C. *A Chemist's Guide to Density Functional Theory*, 2nd ed.; Wiley-VCH: Weinheim, 2001; pp 1−300.

(14) Becke, A. D. *J. Chem. Phys.* **1993**, *98*, 5648−5652.

(15) Lee, C.; Yang, W.; Parr, R. G. *Phys. Rev. B* **1988**, *37*, 785−789.

(16) Jircitano, A. J.; Spudich, T. M.; Ulrich, L.; Saxton, N. L. Penn State Erie, The Behrend College, Erie, PA. Personal communication 2004.

(17) Frisch, M. J.; Trucks, G. W.; Schlegel, H. B.; Scuseria, G. E.; Robb, M. A.; Cheeseman, J. R.; Zakrzewski, V. G.; Montgomery, J. A., Jr.; Stratmann, R. E.; Burant, J. C.; Dapprich, S.; Millam, J. M.; Daniels, A. D.; Kundin, K. N.; Strain, M. C.; Farkas, O.; Tomasi, J.; Barone, V.; Cossi, M.; Cammi, R.; Mennucci, B.; Pomelli, C.; Adamo, C.; Clifford, S.; Ochterski, J.; Petersson, G. A.; Ayala, P. Y.; Cui, Q.; Morokuma, K.; Malick, D. K.; Rabuck, A. D.; Raghavachari, K.; Foresman, J. B.; Cioslowski, J.; Ortiz, J. V.; Stefanov, B. B.; Liu, G.; Liashenko, A.; Piskorz, P.; Komaromi, I.; Gomperts, R.; Martin, R. L.; Fox, D. J.; Keith, T.; Al-Laham, M. A.; Peng, C. Y.; Nanayakkara, A.; Gonzalez, C.; Challacombe, M.; Gill, P. M. W.; Johnson, B.; Chen, W.; Wong, M. W.; Andres, J. L.; Gonzalez, C.; Head-Gordon, M.; Replogle, E. S.; Pople, J. A. *Gaussian 98, Revision A.11*; Gaussian, Inc.: Pittsburgh, PA, 1998.

(18) Frisch, M. J.; Trucks, G. W.; Schlegel, H. B.; Scuseria, G. E.; Robb, M. A.; Cheeseman, J. R.; Montgomery, J. A., Jr.; Vreven, T.; Kudin, K. N.; Burant, J. C.; Millam, J. M.; Lyengar, S. S.; Tomasi, J.; Barone, V.; Mennucci, B.; Cossi, M.; Scalmani, G.; Rega, N.; Petersson, G. A.; Nakatsuji, H.; Hada, M.; Ehara, M.; Toyota, K.; Fukuda, R.; Hasegawa, J.; Ishida, M.; Nakajima, T.; Honda, Y.; Kitao, O.; Nakai, H.; Klene, M.; Li, X.; Knox, J. E.; Hratchian, H. P.; Cross, J. B.; Bakken, V.; Adamo, C.; Jaramillo, J.; Gomperts, R.; Stratmann, R. E.; Yazyev, O.; Austin, A. J.; Cammi, R.; Pomelli, C.; Ochterski, J. W.; Ayala, P. Y.; Morokuma, K.; Voth, G. A.; Salvador, P.; Dannenberg, J. J.; Zakrzewski, V. G.; Dapprich, S.; Daniels, A. D.; Strain, M. C.; Farkas, O.; Malick, D. K.; Rabuck, A. D.; Raghavachari, K.; Foresman, J. B.; Ortiz, J. V.; Cui, Q.; Baboul, A. G.; Clifford, S.; Cioslowski, J.; Stefanov, B. B.; Liu, G.; Liashenko, A.; Piskorz, P.; Komaromi, I.; Martin, R. L.; Fox, D. J.; Keith, T.; Al-Laham, M. A.; Peng, C. Y.; Nanayakkara, A.; Challacombe, M.; Gill, P. M. W.; Johnson, B.; Chen, W.; Wong, M. W.; Gonzalez, C.; Pople, J. A. *Gaussian 03, Revision D.01*; Gaussian, Inc.: Wallingford, CT, 2004.

(19) Hay, P. J.; Wadt, W. R. *J. Chem. Phys.* **1985**, *82*, 299−310.

(20) Ohanessian, G.; Brusich, M. J.; Goddard, W. A., III *J. Am. Chem. Soc.* **1990**, *112*, 7179−7189.

(21) Dennington, R. II.; Keith, T.; Millam, J.; Eppinnett, K.; Hovell, W. L.; Gilliland, R. *GaussView, Version 3.09*; Semichem, Inc.: Shawnee Mission, KS, 2003.

(22) Wong, M. W. *Chem. Phys. Lett.* **1996**, *256*, 391−399.

(23) Stratmann, R. E.; Scuseria, G. E.; Frisch, M. J. *J. Chem. Phys.* **1998**, *109*, 8218−8224.

(24) Basolo, F.; Pearson, R. G. *Mechanisms of Inorganic Reactions: A Study of Metal Complexes in Solution*; Wiley & Sons: New York, 1967; pp 351−453.

(25) Wilkins, R. G. *The Study of Kinetics and Mechanism of Reactions of Transition Metal Complexes*; Allyn & Bacon: Boston, MA, 1974; pp 223−225.

(26) Nakamoto, K. *Infrared and Raman Spectra of Inorganic and Coordination Compounds. Part B: Applications in Coordination, Organometallic, and Bioinorganic Chemistry*, 5th ed.; Wiley & Sons: New York, 1997; pp 58−59.

(27) Pople, J. A.; Schlegel, H. B.; Raghavachari, K.; DeFrees, D. J.; Binkley, J. F.; Frisch, M. J.; Whitesides, R. F.; Hout, R. F.; Hehre, W. J. *Int. J. Quantum Chem Symp.* **1981**, *15*, 269−278.

(28) Scott, A. P.; Radom, L. *J. Phys. Chem.* **1996**, *100*, 16502−16513.

(29) *CRC Handbook of Chemistry and Physics*, 70th ed.; Weast, R. C., Lide, D. R., Astle, M. J., Beyer, W. H., Eds.; CRC Press: Boca Raton, FL, 1989; p D-61.

(30) Coe, J. S. *MTP Int. Rev. Sci.: Inorg. Chem., Ser. 2* **1974**, 45−62.

(31) Cooper, J.; Ziegler, T. *Inorg. Chem.* **2002**, *41*, 6614−6622.

(32) Turro, N. J. *Modern Molecular Photochemistry*; University Science Books: Sausalito, CA, 1991; pp 72−74.

(33) Yersin, H.; Humbs, W.; Strasser, J. *Coord. Chem. Rev.* **1997**, *159*, 325−358.

(34) Balashev, K. P.; Puzyk, M. V.; Kotlyar, V. S.; Kulikova, M. V. *Coord. Chem. Rev.* **1997**, *159*, 109−120.

(35) Yersin, H.; Strasser, J. *Coord. Chem. Rev.* **2000**, *208*, 331−364.

(36) Hissler, M.; McGarrah, J. E.; Connick, W. B.; Geiger, D. K.; Cummings, S. D.; Eisenberg, R. *Coord. Chem. Rev.* **2000**, *208*, 115−137.

(37) Yersin, H.; Donges, D. *Top. Curr. Chem.* **2001**, *214*, 81−186.

(38) Castellano, F. N.; Pomestchenko, I. E.; Shikhova, E.; Hua, F.; Muro, M. L.; Rjapkse, N. *Coord. Chem. Rev.* **2006**, *250*, 1819−1828.

CT700158G